Supporting Information

Toward enhanced photocatalytic activity of graphite carbon nitride through rational design of noble metal-free dual cocatalyst

Ling-Zhi Qin,†[a] Ye-Zhan Lin,†[a] Yi-Chuan Dou,[a] Yi-Jin Yang,[a] Kui Li,[a]* Tao Li[b*] and Fu-Tian Liu[a]

[a]School of Materials Science and Engineering, University of Jinan, Jinan 250022, China.
[b]Engineering Technology Research Center of Henan Province for Solar Catalysis,School of Chemistry and Pharmaceutical Engineering, Nanyang Normal University, Nanyang, Henan, China.

Email: mse_lik@ujn.edu.cn, ltao84@163.com

† These two authors contribute equally to this work.

Supporting Figures.

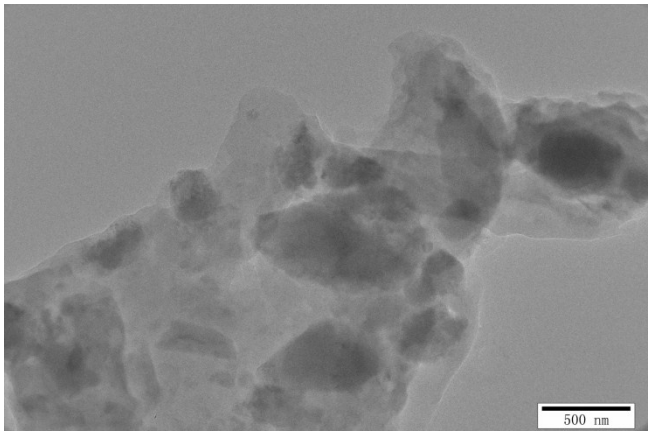

Fig. S1. Transmission electron microscopy (TEM) image of the g-C_3N_4-$Ni(OH)_2$.

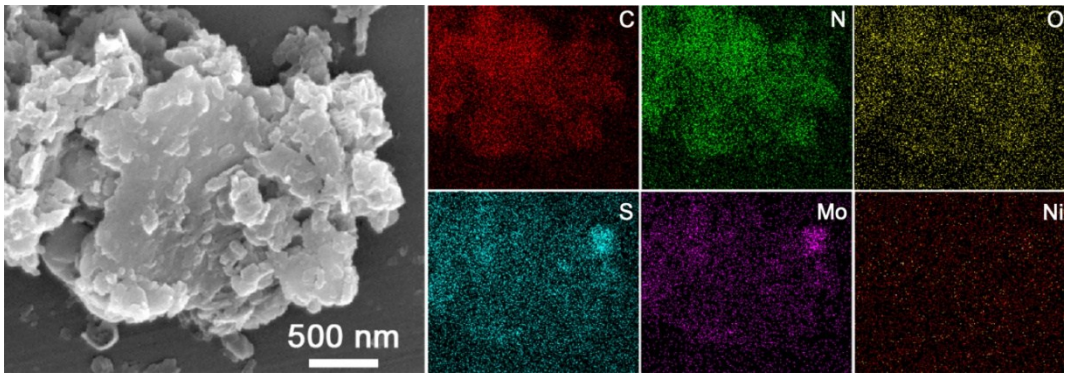

Fig. S2. The elemental mapping image of the optimal g-C_3N_4-MoS_2-$Ni(OH)_2$.

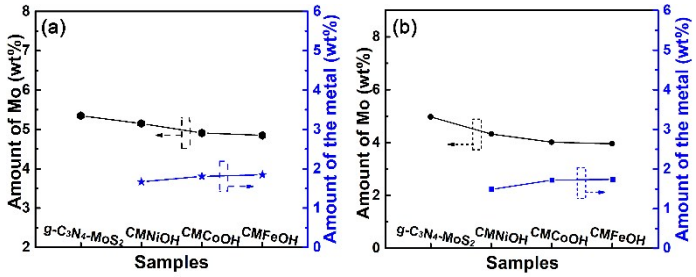

Fig. S3 (a) The amount of Mo and Ni, Co, Fe concentrations tested via the ICP and (b) the surface contents of metals via the XPS of the g-C_3N_4-MoS_2, g-C_3N_4-MoS_2-$Ni(OH)_2$ (CMNiOH), g-C_3N_4-MoS_2-$Co(OH)_2$ (CMCoOH), g-C_3N_4-MoS_2-$Fe(OH)_3$ (CMFeOH), respectively.

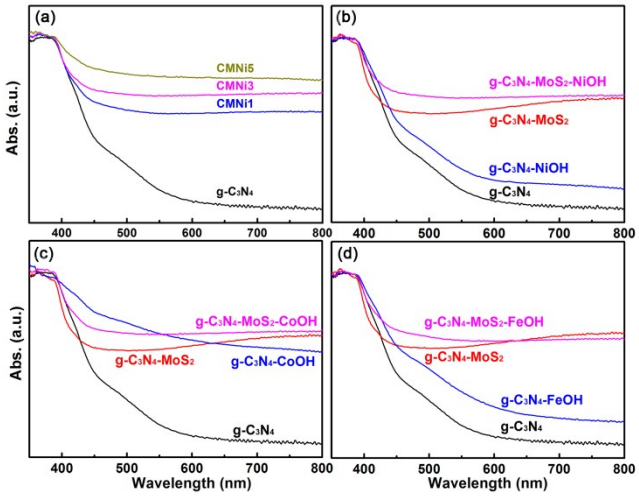

Fig. S4. (a) Effect of amount of $Ni(OH)_2$ on the UV−visible diffuse reflection spectra in g-C_3N_4-MoS_2-$Ni(OH)_2$. The comparison results of the UV−visible diffuse reflection spectra of g-C_3N_4, g-C_3N_4-$M(OH)_x$, g-C_3N_4-MoS_2, and g-C_3N_4-MoS_2-$M(OH)_x$, with M of (b) $Ni(OH)_2$, (c) $Co(OH)_2$ and (d) $Fe(OH)_3$.

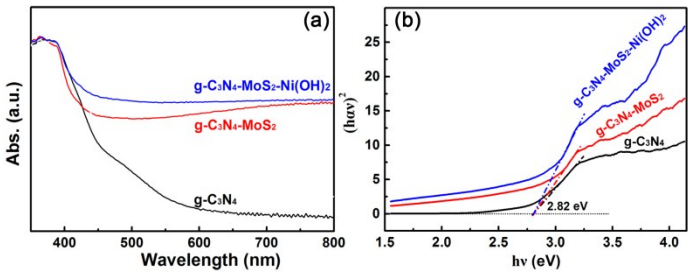

Fig. S5. The (a) UV−visible diffuse reflection spectra and (b) the band gaps of the g-C_3N_4, g-C_3N_4-MoS_2 with and without $Ni(OH)_2$.

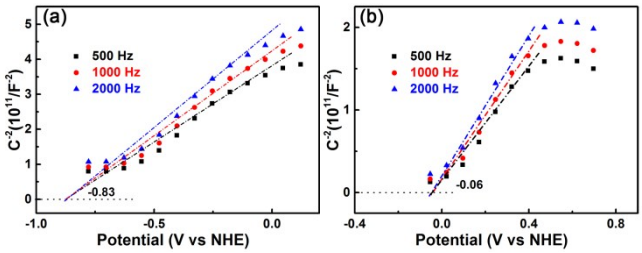

Fig. S6. The Mott–Schottky plots of (a) $Co(OH)_2$ and (b) $Fe(OH)_3$.

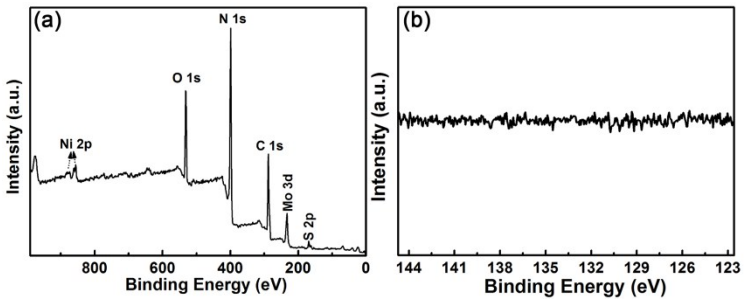

Fig. S7. (a) Survey XPS spectrum of the g-C_3N_4-MoS_2-$Ni(OH)_2$ ternary heterostructure and (b) high-resolution XPS spectra of P 2p. It could be observed that there was no P in the resultant heterostructure sample.

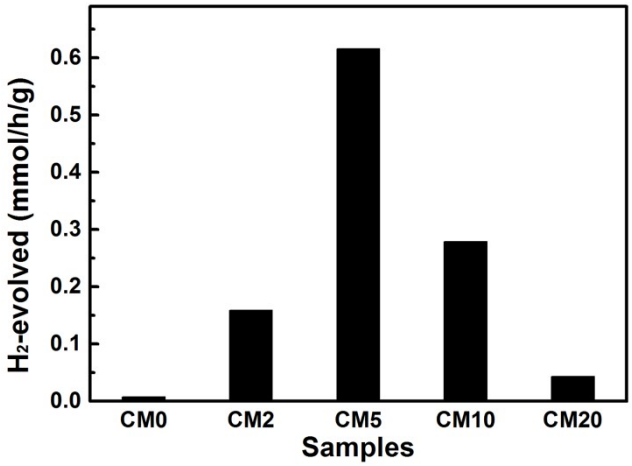

Fig. S8. The photocatalytic hydrogen production rate of the g-C_3N_4-MoS_2 with different amount of MoS_2.

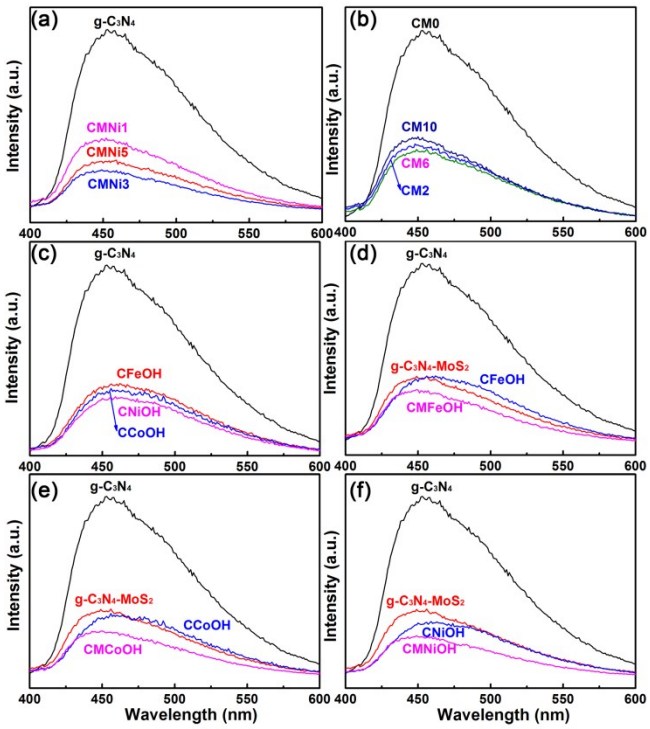

Fig. S9. The PL spectra of the g-C_3N_4-based samples with different amount of $Ni(OH)_2$, (b) MoS_2, and (c) types of $M(OH)_x$. The comparsion results of the PL spectra of g-C_3N_4, g-C_3N_4-MoS_2 with and without (d) $Fe(OH)_3$, (e) $Co(OH)_2$ and (f) $Ni(OH)_2$.

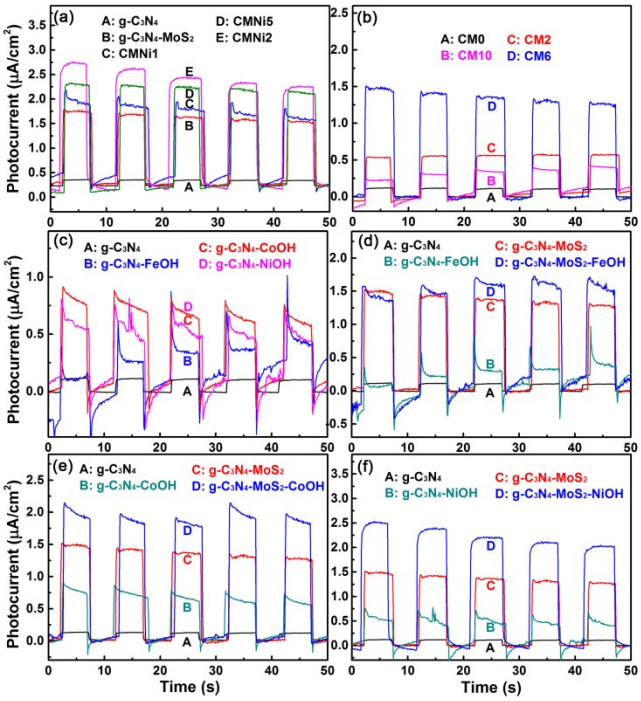

Fig. S10. The transient photocurrent responses of the g-C_3N_4-based samples with different amount of $Ni(OH)_2$, (b) MoS_2, and (c) types of $M(OH)_x$. The comparsion results of the transient photocurrent responses of g-C_3N_4, g-C_3N_4-MoS_2 with and without (d) $Fe(OH)_3$, (e) $Co(OH)_2$ and (f) $Ni(OH)_2$.

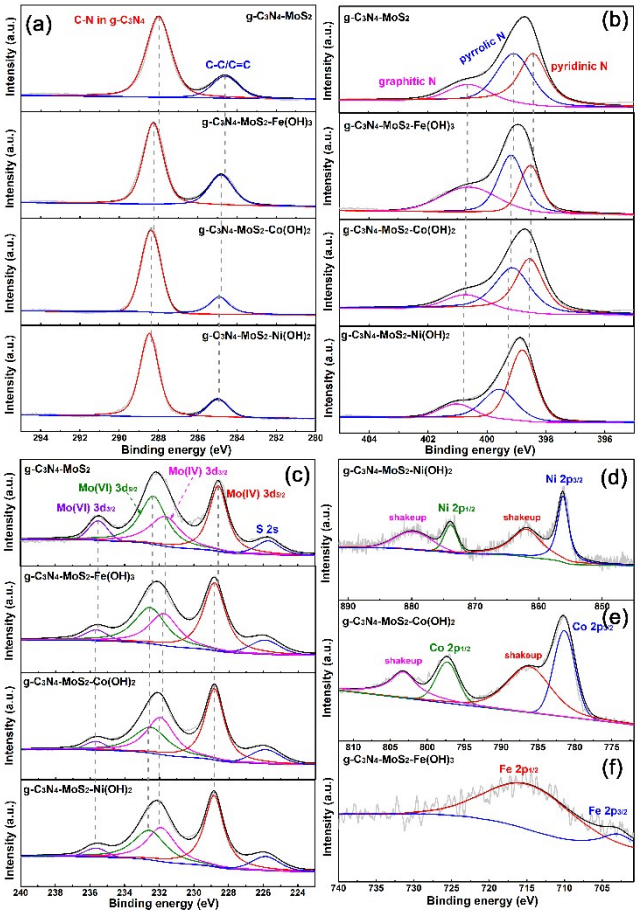

Fig. S11 The high-resolution XPS spectra of (a) C 1s, (b) N 1s, (c)Mo 3d, (d) Ni 2p, (e) Co 2p and (f) Fe 2p of the optimal g-C_3N_4-MoS_2 and g-C_3N_4-MoS_2-$M(OH)_x$ ternary heterostructures.